C. R. Mecanique 346 (2018) 460–476

Contents lists available at ScienceDirect

Comptes Rendus Mecanique

www.sciencedirect.com

Influence of particle shape on the microstructure evolution and the mechanical properties of granular materials

Jianqiu Tian [a], Enlong Liu [a,b,*], Lian Jiang [a], Xiaoqiong Jiang [a], Yi Sun [a], Ran Xu [c]

[a] State Key Laboratory of Hydraulics and Mountain River Engineering College of Water Resource & Hydropower, Sichuan University, Chengdu 610065, China

[b] Northwest Institute of Eco-Environment and Resources, State Key Laboratory of Frozen Soil Engineering, Chinese Academy of Sciences, Lanzhou, Gansu 730000, China

[c] Institution of Disaster Management and Reconstruction, Sichuan University, Chengdu 610207, China

ARTICLE INFO

Article history:
Received 10 November 2017
Accepted 24 March 2018
Available online 5 April 2018

Keywords:
Particle shape
Direct shear simulation
Particle rotation
Fabric evolution
Average path length
Rowe's stress–dilatancy

ABSTRACT

In order to study the influence of particle shape on the microstructure evolution and the mechanical properties of granular materials, a two-dimensional DEM analysis of samples with three particle shapes, including circular particles, triangular particles, and elongated particles, is proposed here to simulate the direct shear tests of coarse-grained soils. For the numerical test results, analyses are conducted in terms of particle rotations, fabric evolution, and average path length evolution. A modified Rowe's stress–dilatancy equation is also proposed and successfully fitted onto simulation data.

1. Introduction

Granular materials exist in nature and human activities extensively, such as debris-flow in nature and rockfill materials in civil engineering. Their strength and deformation vary with the different particle shapes. The physical mechanisms responsible for these differences are a question often raised by many researchers [1–5], from which we can see that the mechanisms also need to be explored through different perspectives and methods. Therefore, the particle shape is still worth noting, and its influence on the mechanical behaviour of granular materials remains an open topic.

Laboratory experiments have been carried out to explore the influence of particle shape on the mechanical properties of granular assemblies by many researchers, such as Shinohara et al. [6], Cho et al. [7], and Yang et al. [8]. However, these traditional laboratory experiments (such as direct shear tests, simple shear tests, and triaxial tests) only provide limited macroscopic strength and deformation. To collect microscopic information about the specimens, X-rays [9], CT scan [10], photoelasticity [11] and so on were employed in laboratory tests. But these methods are extremely expensive. Therefore, a cheaper technique, discrete element method (DEM), was employed by many researchers [12]; it has also other advantages, such as having access to any microscopic data including contact forces and controlling different loading-paths easier. DEM could also be used to investigate the relationship between microscopic information and the macromechanical properties of granular assemblies [13]. With the help of DEM, the microscopic information of a specimen is collected more easily than

* Corresponding author at: Northwest Institute of Eco-Environment and Resources, State Key Laboratory of Frozen Soil Engineering, Chinese Academy of Sciences, Lanzhou, Gansu 730000, China.

E-mail addresses: liuenlong@lzb.ac.cn, liuenlong@scu.edu.cn (E. Liu).

https://doi.org/10.1016/j.crme.2018.03.006
1631-0721/

before. At the same time, with an improved computational efficiency, the non-circular and non-spherical shapes can be considered in the DEM. Hence, many numerical simulations for researching the role of particle shape in granular materials were performed. For instance, Nouguier-Lehon et al. [14], using biaxial numerical simulation to explore different shapes (i.e. circular, isotropic polygonal, and elongated polygonal shapes) showed that the behaviour of samples with isotropic particles can be dissociated from that of samples with anisotropic particles. Zhao et al. [15] developed four categories of assemblies with different angularities to investigate the evolution of coordination number, contact force distribution, and anisotropies of particle orientation and contact normal by the YADE DEM code. Yang et al. [5] performed undrained numerical simulation to study the differences between three types of non-convex grains (i.e. disk, ellipse, and triangle) without rolling resistance and disks with rolling resistance, demonstrating that the influence of the shape irregularity of particles is much different from that of the rolling resistance at the particle contact. In previous works [16–18], some other characters of particle shape have been studied by using DEM. From these references, particle shape was systematically accounted for through anisotropy and coordination numbers. This is however too rough in some cases and more information can be recovered for instance by considering particle rotation and complex networks. Complex network has been used in the analysis of granular materials [19,20]; nevertheless, only one shape of particles was used in numerical simulations with circular or spherical particles. Hence, using a complex network to analyse the role of particle shape in granular materials is a new way.

There is an increasing interest in quantifying the interactions between particles, as evidenced by publications, including those by Thornton et al. [21], Kuhn [22], and Wang et al. [23]. Furthermore, information about particle contact in connection with the macromechanical properties of granular materials has been studied by researchers in many ways. For instance, Kruyt [24] investigated the relations between macro-level, continuum characteristics and micro-level, particle characteristics, and an evolution relation was proposed for the changes in the fabric tensor as a function of the fabric tensor and the strain increment tensor, which agreed well with the simulations. Nicot et al. [25] proposed two micromechanical models that agree well with the results from numerical simulations containing 10,000 spherical particles. Other researchers, including Chang et al. [26] and Zhao et al. [27], also tried to establish the relationship between fabric evolution and the macro mechanical behaviour of granular materials. There were few non-circular particles considered in the existing researches to establish the bridge between micro-information and the macrobehaviour of granular materials. Hence, in this paper we will propose a two-dimensional DEM analysis of different particle shapes and try to establish a bridge between the micro and macro property.

In recent researches [14–18], most of them have been focused on investigating the influence of particle shape on the micro-scale information through a traditional method (i.e. fabric evolution). The influence of particle shape on granular materials explored from other perspectives and methods is relatively lacking. On the other hand, establishing the bridge between micro-analysis and macrobehaviour just considers the circular or spherical particles in major related references. Particle shape received little attention in most analyses aimed at establishing the bridge between micro- and macroproperties. It is obvious that the influence of particle shape on the microstructure evolution and the mechanical properties of granular materials is still an open topic, and many works can be done on this. In this paper, we propose a two-dimensional DEM analysis of different granular materials: circular particles, triangular particles, and elongated particles. Firstly, the particle shape measurement is introduced to identify the particles used in numerical simulations. Secondly, the simulated method of direct shear tests is proposed to do the numerical simulations. Then, influences of particle shape on macromechanical properties, particle rotation, fabric and average path length are analysed, respectively. Finally, the Rowe's stress–dilatancy relation is modified according to particle shape and fabric, and this modified equation is compared with the numerical results.

2. Particle shape measurement and structural characteristics

2.1. Particle shape measurement

The aspect ratio (AR), convexity (C) and sphericity (S) proposed by Yang and Altuhafi [1,28] are adopted to measure the particle shape, referring to Fig. 1a. The aspect ratio is defined as the ratio between the minimum and maximum Feret diameters, where the Feret diameter of the particle is defined as the measured distance between parallel lines tangent to an object's outline; the convexity is the area of the particle (A) divided by its area if any concavity within its perimeter is filled ($A + B$); the sphericity is defined as the ratio of the perimeter of a circle with the same area as the area of the particle to its actual perimeter. From the definitions of the aspect ratio, convexity and sphericity [28], we know that the three methods consider the influence of different factors on the shape. AR is sensitive to the elongation of the particle; C controls the concavity of the particle; S is a parameter comparing particles with circles. The whole information about particle shape cannot be described using one or two of them [28], and the weighted coefficients of these three parameters are still not clear. Therefore, by combining AR, C, and S, a new shape measurement, the overall regularity (OR), is defined as the average of the three shape parameters proposed as [1]:

$$OR = (AR + C + S)/3 \tag{1}$$

Using this method to calculate the three types of particle, the OR values for circular, triangular and elongated particles are determined as 1.0, 0.96, and 0.79, respectively. Such process is illustrated in Fig. 1b.

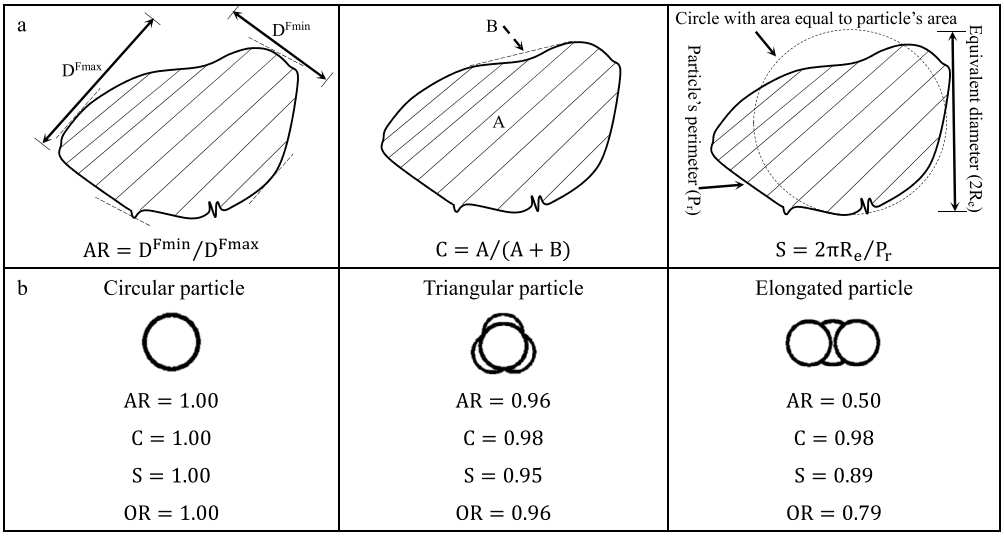

Fig. 1. Particle shape measurement: (a) Definition of shape parameters (*OR*); (b) calculation of the *OR* of three different particles. Note: $OR = (AR + C + S)/3$.

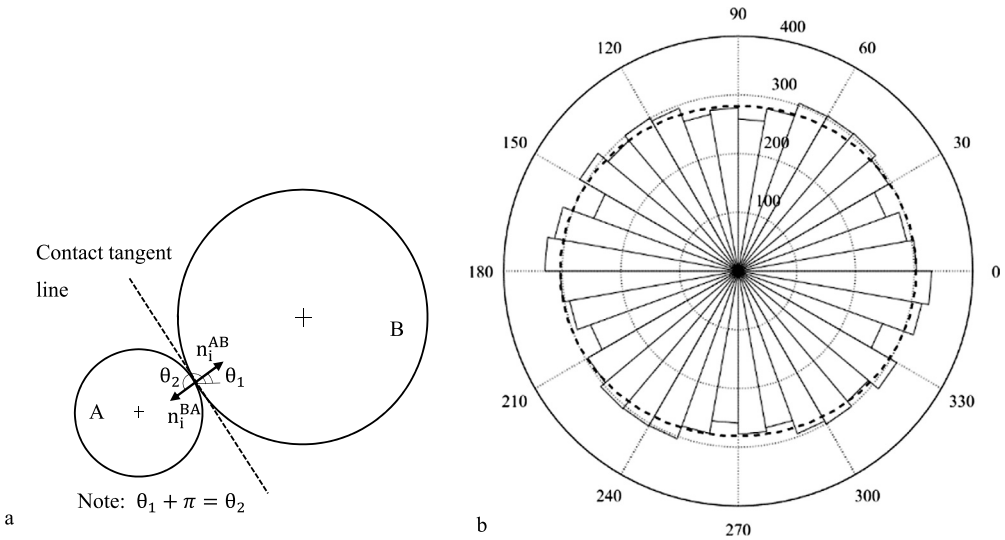

Fig. 2. Schematic diagram of fabric: (a) orientations of the contact normal; (b) illustrating a rose diagram and using equation (2) to approximate it.

2.2. Characteristics of the fabric

For analysing the contact properties between soil particles upon loading, the characteristics of the fabric are presented here. The contacts of the grains are illustrated in Fig. 2a, where the orientations θ_1 and θ_2 both represent the contact directions of particles A and B. The rose diagram in Fig. 2b characterizes the contact orientation with an angular interval of 10 degrees. The polar axis represents the contact numbers. Rothenburg and Bathurst [29] proposed an approximation of the normalized contact orientation distribution, which can be obtained based on a second Fourier component, as follows:

$$E(\theta) = \left[1 + a\cos 2(\theta - \theta_a)\right]/2\pi \tag{2}$$

where a is a parameter describing the magnitude of anisotropy in contact orientations, θ_a is the direction of anisotropy, and θ is the orientation for the contacts between grains. When $a = 0$ the normalized contact orientation distribution is isotropic. Equation (2) is used to approximate a rose diagram and the approximated line is drawn as a dash line in Fig. 2b.

The coordination number (Z) [24] is the average contact number of a particle in a particle assembly, shown as follows:

$$Z = 2N_c/N_p \tag{3}$$

where N_c represents all contact numbers, and N_p stands for all particle numbers.

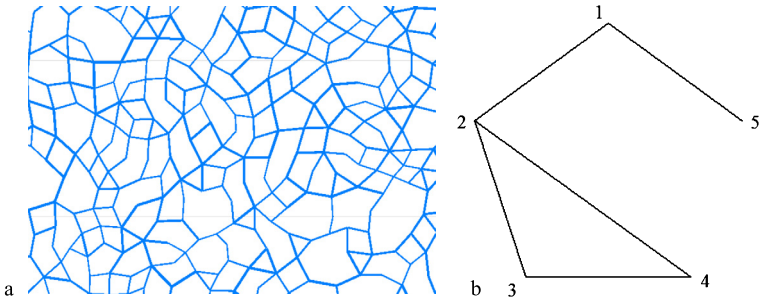

Fig. 3. Illustration of the network for the assembly of particles: (a) the local network of the assembly; (b) a simple network containing five nodes.

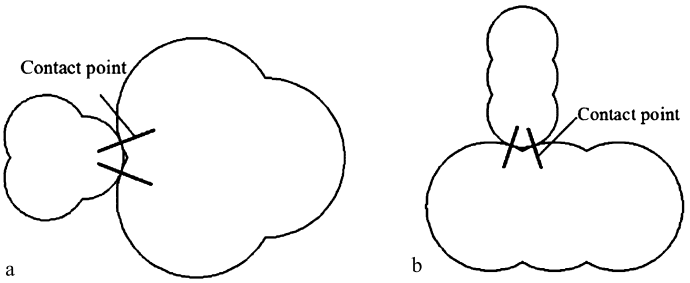

Fig. 4. Contacts between particles: (a) contacts between triangular particles; (b) contacts between elongated particles.

2.3. The characteristic of network

The assembly of particles can be treated as a network (see Fig. 3a), so definitions in complex network are introduced to describe their structural properties in which the average path length (L) [30] can represent the connectivity of network, proposed as:

$$L = 1/\left[N(N-1)\right] \times \sum_{i \neq j} d_{ij} \tag{4}$$

where d_{ij} is the number of edges in the shortest path between nodes i and j, and N is the number of nodes in the network. The denominator (i.e. $N(N-1)$) represents the sum of the numbers of edges in the shortest path among all nodes in the densest state, while the numerator (i.e. $\sum_{i \neq j} d_{ij}$) represents the sum of numbers of edges in the shortest path among all nodes in a particle assembly.

Fig. 3b shows a simple network that contains five nodes and five edges. From this network, L is calculated as 1.7. It should be noted that there are two or more than two contact points between two irregular particles (see Fig. 4). Such contacts should be treated as one edge when the assembly is treated as a network by considering the definition of the average path length [30].

3. DEM simulation and analysis of the results

3.1. Test preparation

In this paper, the properties of cohesionless specimens are explored through using the program PFC^{2D}, so the relative density (D_r) must be used to compare different specimens. The relationship between relative density and porosity is shown as:

$$D_r = (1 - n_{min})(n_{max} - n)/\left[(1-n)(n_{max} - n_{min})\right] \tag{5}$$

where n_{max} is the maximum porosity, n_{min} is the minimum porosity, and n is the porosity of the specimen. The maximum and minimum porosities can be obtained from the relative density test of coarse-grained soils. And this test refers to specification of soil test [31]. By simulating this test, the maximum and minimum porosities of different particle shapes are obtained first. Then, the specimens' porosities with the same relative density of 70% through Eq. (5) are calculated. The results are displayed in Table 1. From this table, the maximum and minimum porosities decrease with the OR of particle shape becoming smaller. Such changing rule is consistent with results of Nouguier-Lehon and Mirghasemi [14,32]. The model parameters used in simulation of the relative density tests and direct shear tests of coarse-grained soils are shown in Table 2, in which the magnitude of stiffness and particle friction are referred to [5]. In addition, the linear model of PFC^{2D} is

Table 1
Porosity results for different types of specimens.

	Specimen with circular particles	Specimen with triangular particles	Specimen with elongated particles
n_{max}	0.217	0.195	0.165
n_{min}	0.168	0.146	0.118
n	0.183	0.161	0.134

Table 2
Model parameters in DEM simulations.

Parameter	Value
Particle size (radius)	0.2–0.4 mm
Particle density	2630 kg/m^3
Damping coefficient	0.7
Particle friction	0.5
Wall friction	0
Particle/wall normal stiffness	1.5×10^8 N/m
Particle/wall shear stiffness	1.0×10^8 N/m

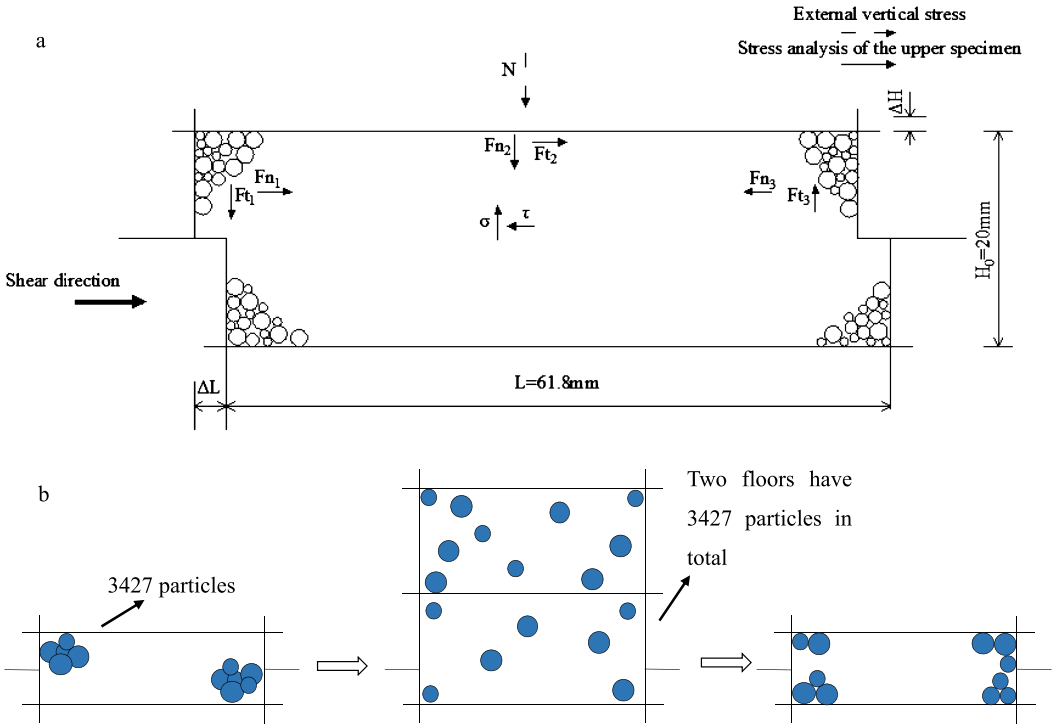

Fig. 5. Illustration of DEM simulation: (a) schematic diagram of the direct shear box; (b) schematic diagram of specimen preparation with circular particles.

used in the numerical tests. The clump command is used to control the particle shape in the numerical simulation of direct shear tests. In the range of particle size, all of particles are drawn from uniform distributions throughout the model domain.

The process of performing the direct shear test is explained here. Firstly, the direct shear box is generated in a domain composed of six rigid walls and two additional flanges. Two flanges are added to prevent particle leakage during shearing. Such direct shear box is illustrated in Fig. 5a. Secondly, specimens are generated in a box with porosity and particle size, introduced in Tables 1 and 2. Attention should be paid that clumps may overlap with each other during this stage. Then, in order to generate clumps without overlap, the top wall is regenerated to amplify the box three times before the specimen is regenerated according to particle number that can be recorded in the previous step (the specimen with circular particles has 3427 grains; the specimen with triangular particles has 3529 grains, and the specimen with elongated particles has 3648 grains. The number of particles is limited by the computational efficiency of DEM and it is large enough to reflect the microstructure and the mechanical properties of granular materials.). At last, the generated particles are divided into two floors, and each floor is compressed to the target porosity separately by walls. This process ceases when the target porosity is achieved. The illustration of specimen preparation refers to Fig. 5b. The direct shear simulations are carried out under different vertical stresses (200 kPa, 400 kPa, and 600 kPa).

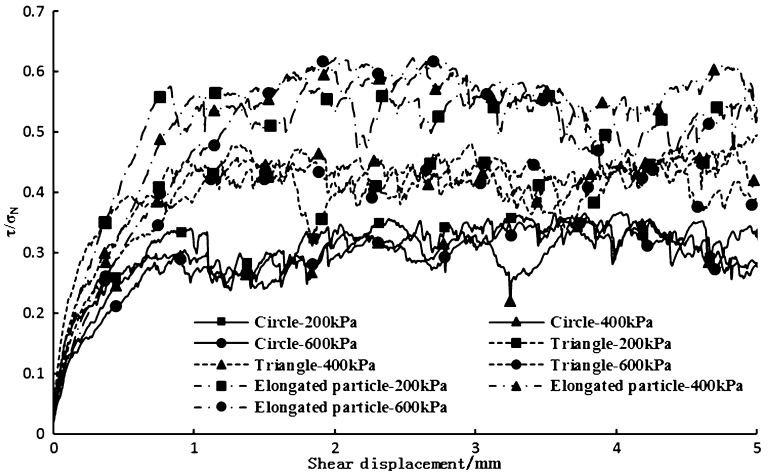

Fig. 6. Relations between shear stress ratio and shear displacement.

3.2. Shearing and data recording

During the shearing stage, the velocity of the top wall is adjusted via a servo-controlled mechanism to maintain a constant vertical stress. The bottom box is applied with a constant velocity of 1 cm/s. In the simulations, the dimensionless number I called the inertia parameter [33–36] is below 3.0×10^{-5} satisfying with $I \ll 1$, so the velocity 1 cm/s is slow enough to ensure quasi-static conditions. The shearing direction is shown in Fig. 5a. Shearing ceases when the shear displacement attains 5 mm.

The vertical and shear displacements can be obtained by recording the displacements of the top wall and the bottom box. The shear stress is calculated by the equation of $\tau \times L = Fn_1 + Ft_2 - Fn_3$, where Fn_1 and Fn_3 can be recorded in the left and right walls of the upper box, Ft_2 being so small compared with Fn_1 and Fn_3 that it can be neglected (this is a consequence of the wall/particle contact law). This method is also used by Thornton et al. [37]. The stress analysis of the upper specimen is illustrated in Fig. 5a.

3.3. Influence of particle shape on the macromechanical properties

Three types of specimens are sheared under different vertical stresses (200 kPa, 400 kPa, and 600 kPa). Fig. 6 shows the shear stress ratio as a function of shear displacement. As we can see in the figure, the curves almost coincide with each other when the specimens have the same particle shape. The specimens with circular particles ($OR = 1.00$) have the lowest values of peak and ultimate shear stress ratio. On the contrary, the specimens with elongated particles ($OR = 0.79$) have the largest values of peak and ultimate shear stress ratio. The values of peak and ultimate shear stress ratio increase when OR decreases. Such a phenomenon can be explained as follows. According to Figs. 2 and 4, there is only one contact point between two circular particles, but there are two or more contact points between two irregular particles. Because the lowest constrains are around the circular particles, the latter can slide more easily than irregular ones. In other words, the specimens with circular particles have the lowest values of peak and ultimate shear stress ratio. The aspect ratio's value (AR) of triangular particles is larger than the one of elongated particles. The higher the value of the aspect ratio, the easier the rolling of the particles. If the particles roll, the contact point will change at the same time. Therefore, the contacts of the triangular particles change more easily than those of the elongated particles do. That is to say, the specimen with triangular particles has the lower values of peak and ultimate shear stress ratio compared with the specimen with elongated particles.

Fig. 7 shows the vertical displacement varying with the increasing shear displacement of three types of granular materials. The ultimate vertical displacement increases with decreasing the vertical stress for the specimen with the same particle shape. On the other hand, the ultimate vertical displacement increases with decreasing OR under the same vertical stress. The vertical displacement is made up of sliding and rolling between particles. And the vertical displacements of different particle shapes are mainly due to different rolling types. If the aspect ratio's value (AR) of the particle decreases, more space is needed when the particles roll. So, the ultimate vertical displacement increases with decreasing AR under the same vertical stress.

3.4. Particle rotation

Particle rotation is an important role representing the motion of particles, especially within the zone near the shear plane. Such a description of particle caught the eyes of researchers, as evidenced by references [38–40]. Therefore, it is interesting to carry out an observational investigation into particle rotation for the three types of assemblies.

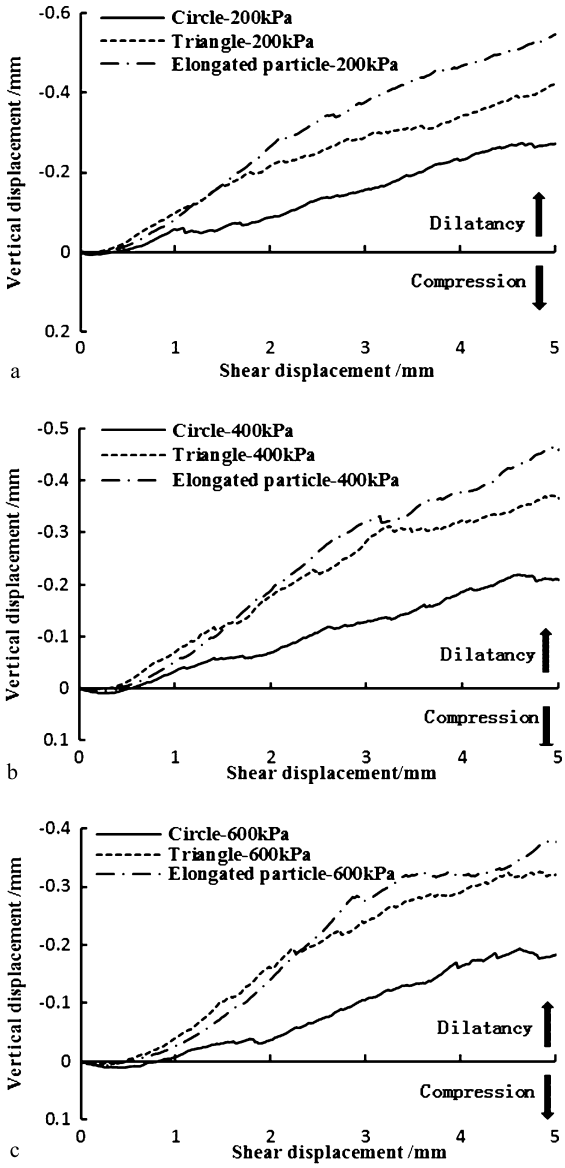

Fig. 7. Relations between vertical displacement and shear displacement: (a) vertical stress 200 kPa; (b) vertical stress 400 kPa; (c) vertical stress 600 kPa.

Fig. 8 shows the evolution of particle rotation in the three types of assemblies under a vertical stress of 200 kPa. In this figure, the bluer the particles, the larger the angle of clockwise rotation. On the other hand, the redder the particles, the larger the angle of anticlockwise rotation. The rotations for three types of particles all begin from two ends of shear plane at *shear displacement* = 1 mm. And the particles on the shear plane gradually begin to rotate with increasing the shear displacement, which is in an agreement with the reference [38]. This phenomenon suggests a disturbed position of the specimen starting from the local zones that are the ends of the shear plane, and gradually spreading out.

The distributions of the average particle rotation for the three types of assemblies are recorded according to the specimen's height, as illustrated in Fig. 9a. In this figure, the average particle rotation near the shear plane is greater than the value far from the shear plane, which agrees with the published results [38]. By comparing the average particle rotation of three types for assemblies, it can be seen that the more regular the particles, the larger the value of the average particle rotation near the shear plane. This phenomenon suggests that the particles with a larger angularity in the specimen cannot rotate easily. Thus, the contacts of the particles are steadier with decreasing the parameter *OR*. In addition, Fig. 9b shows the maximum particle rotation for three types of granular materials. As we can see, the absolute values for the maximum particle rotation increase when the parameter *OR* increases. This trend of curves demonstrates that the more angular the particles, the harder the rotation of the particle in the specimen one more time.

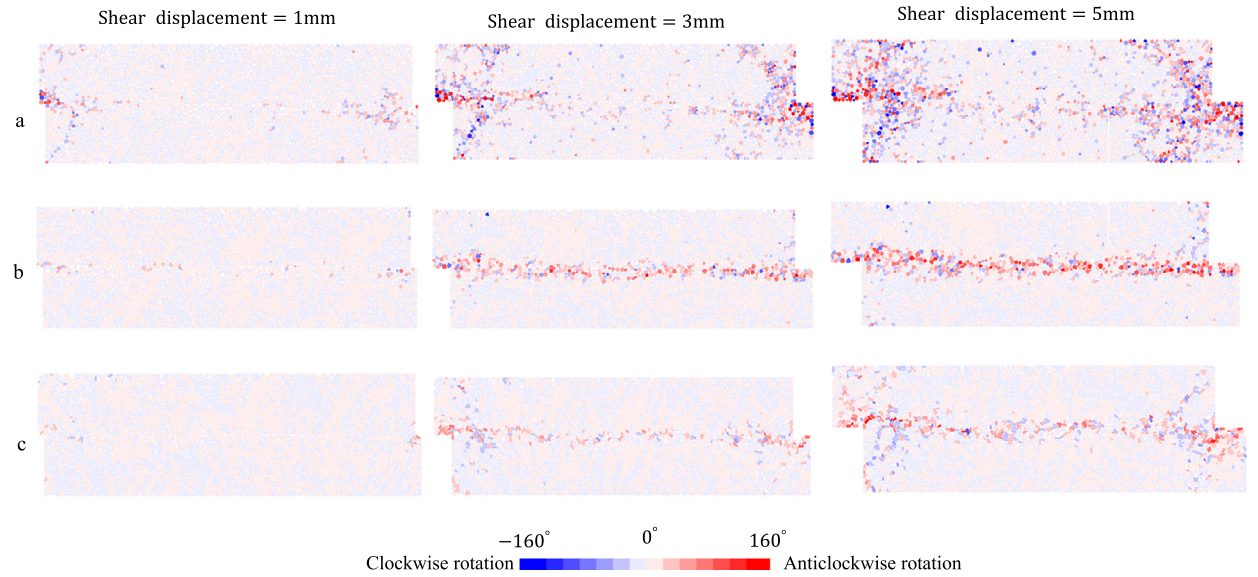

Fig. 8. Particle rotation under a vertical stress of 200 kPa: (a) samples with circular particles; (b) samples with triangular particles; (c) samples with elongated particles.

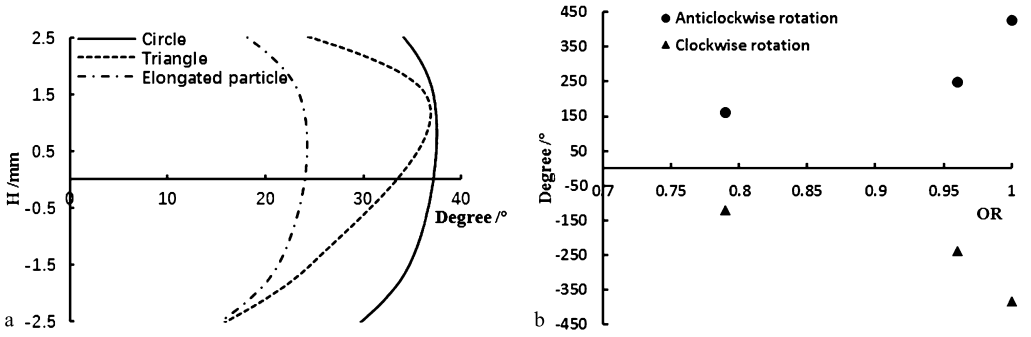

Fig. 9. Statistic of particle rotation at the ultimate state under a vertical stress of 200 kPa: (a) distribution of the average particle rotation along the specimen's height; (b) maximum values of anticlockwise and clockwise rotation for three types of assemblies.

3.5. Fabric evolution with different particle shapes

Fig. 10 illustrates the evolution of anisotropy in contact orientations expressed in terms of the parameter a in Eq. (2). In the initial stage, if the specimens are constituted of circular or triangular particles, the contact distribution is almost isotropic. Such isotropy gradually turns to be anisotropic with increasing the shear displacement. At last, the anisotropy of triangular particles at the ultimate state is greater than that of circular particles. On the other hand, the specimen with elongated particles is anisotropic at the beginning of shear loading. Such anisotropy decreases with increasing the shear displacement, and the value of anisotropy at the ultimate state is the largest among the three types of granular materials. Such a phenomenon can be explained as follows. The isotropy in the initial stage is due to the isotropic particles (circular and triangular grains) distributed in the model domain randomly, as illustrated in Figs. 11a, 11c, 12a, 12c, 13a, and 13c. On the contrary, because there is a main axis in the elongated particles, many contacts are distributed in vertical orientation, as illustrated in Fig. 14. Such contacts distribution result in anisotropy that $a = 0.457$ and $\theta_a = 1.524$, as shown in Fig. 11e. At the ultimate stage, the direction of force transmission turns to an inclined direction, so the contact distribution inclines to the same direction, indicated by Figs. 11b, 11d, 11f, 12b, 12d, 12f, 13b, 13d, and 13f. When the old contact orientations gradually turn to the same direction, the values of anisotropy for specimens consisting of circular or triangular particles increase. On the contrary, the contacts in the specimen constituted of elongated particles are distributed more randomly than before, so the anisotropy gradually decreases, see Figs. 10a–c.

Fig. 15 illustrates the evolution of coordination numbers expressed in terms of the parameter Z. All the coordination numbers decrease with increasing the shear displacement when dilatancy occurs, because the dilatant volumes of specimens lead to a decrease in the contact numbers. Different particles contact conditions are illustrated in Figs. 2 and 4. When the coordination numbers are considered, every contact for triangular and elongated particles is counted. Therefore, the coordination numbers with irregular particles will be bigger than the one computed for circular particles. On the other

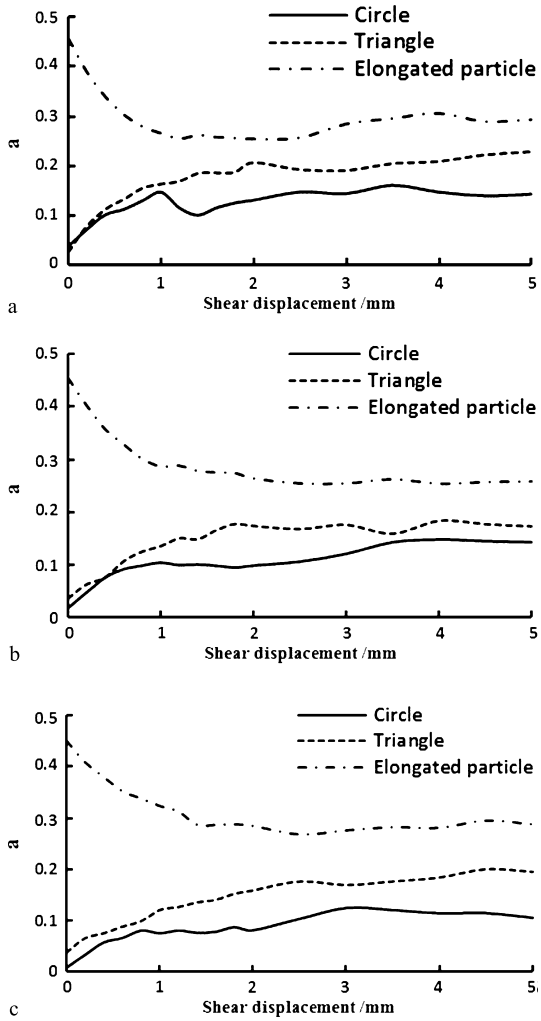

Fig. 10. Anisotropy evolution of granular materials: (a) vertical stress of 200 kPa; (b) vertical stress of 400 kPa; (c) vertical stress of 600 kPa.

hand, the contacts of elongated particle are hard to roll, because the elongated particle has a main axis. In the initial state, the numbers of contact disruption are less than that of the contact creation, so the value of Z increases. Then, when the numbers of contact disruption are larger than those of the contact creation, the value of Z decreases gradually.

3.6. Evolution of the average path length with different particle shapes

If forces between particles are ignored, the specimen can be simplified to a network in which nodes and edges represent particles and contacts, respectively. The properties of the network are studied through complex network. Such theory is now also used in social, biological, computer systems, and in granular materials [19,41–45]. In complex networks, the average path length (*APL*) is an important parameter for measuring message delivery and connectivity [46]. So, it is proposed to describe the evolution of the network in the direct shear test exploring the micro-property further.

Fig. 16 shows the evolution of *APL* under different vertical stresses during shearing. The values of *APL* all decrease firstly and then increase. This trend is similar to the relationship between the vertical displacement and the shear displacement. But the lowest point of *APL* falls behind the point where dilatancy starts. As we can see, if the specimen is compressed, the particles among the contacts gradually increase (i.e. edges are increasing in the network). So, the connectivity is better than before, and the value of *APL* gradually decreases. If the specimen is dilatant, the value of *APL* increase. Furthermore, such trend of *APL* is contrary to that of Z and is more sensitive to the variation of the specimen than Z.

By comparing the values of *APL* for the three categories of granular materials at the same shear strain level, it can be seen that the values of *APL* for isotropic particles are larger than that for elongated particles. This phenomenon suggests that the connectivity of elongated particles is better than that of isotropic particles. In other words, if there are two or more contact points between two particles, they are treated as one edge when the specimen is considered as a network. The circular and triangular particle have similar structures in the network, and the elongated particle has a denser structure than isotropic

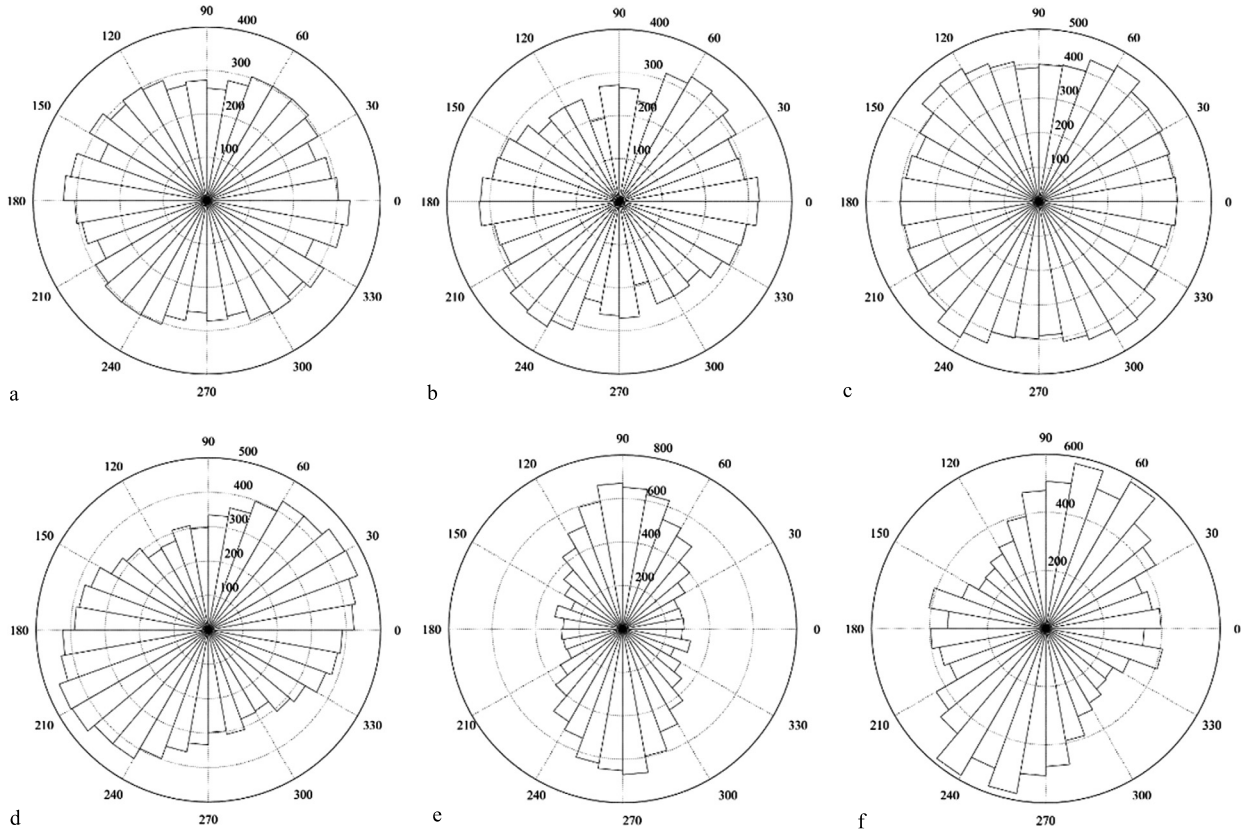

Fig. 11. Rose diagrams of contacts orientation under a vertical stress of 200 kPa: (a) initial state of the circular grains; (b) ultimate state of the circular grains; (c) initial state of the triangular grains; (d) ultimate state of the triangular grains; (e) initial state of the elongated grains; (f) ultimate state of the elongated grains.

particles. By combining the evolution of Z, it can be seen that, on the structure scale, the isotropic particles are similar to each other, but that there are differences between circular and triangular particles when the contact information is taken into account. The elongated particle is different from the isotropic particle on the structure and contact scales, and the minimum of L is after the maximum of Z. It can be seen that the structure of the specimen is disturbed when many contacts are disturbed. And combining L with Z can describe the shear strengths of the three categories of assemblies. The better connectivity is and the more contacts of specimens there are, the larger the values of the peak and ultimate shear stress ratio will be.

4. The revised Rowe's stress–dilatancy relation considering particle shape

Rowe [47] introduced a stress–dilatancy relationship for granular materials based on the minimum energy ratio principle. Such a relationship is formulated as:

$$-\frac{\sigma_1 \dot{\varepsilon_1}}{\sigma_3 \dot{\varepsilon_3}} = \overline{E}_{\min} \tag{6}$$

and

$$\overline{E}_{\min} = \tan^2\left(\frac{\pi}{4} + \frac{\varphi_\mu}{2}\right) \tag{7}$$

In Equation (6), σ_1 and σ_3 are the major and minor principal stresses respectively, $\dot{\varepsilon_1}$ and $\dot{\varepsilon_3}$ are the major and minor principal strain rates, respectively, and $\overline{E}_{\min}$ is the work ratio. In Equation (7), φ_μ is the angle of friction between the particles. Gutierrez et al. [48] derived a non-coaxial version of Rowe's stress–dilatancy relation by turning the direction of the principal strain rate to the direction of the principal stress. Then φ_μ takes the place of φ_c. Finally, combining Equation (6), the non-coaxial version of Rowe's stress–dilatancy relationship is revised as [48]:

$$\cos 2\Delta \sin\psi = \frac{\sin\varphi_c - \sin\varphi}{1 - \sin\varphi \sin\varphi_c} \tag{8}$$

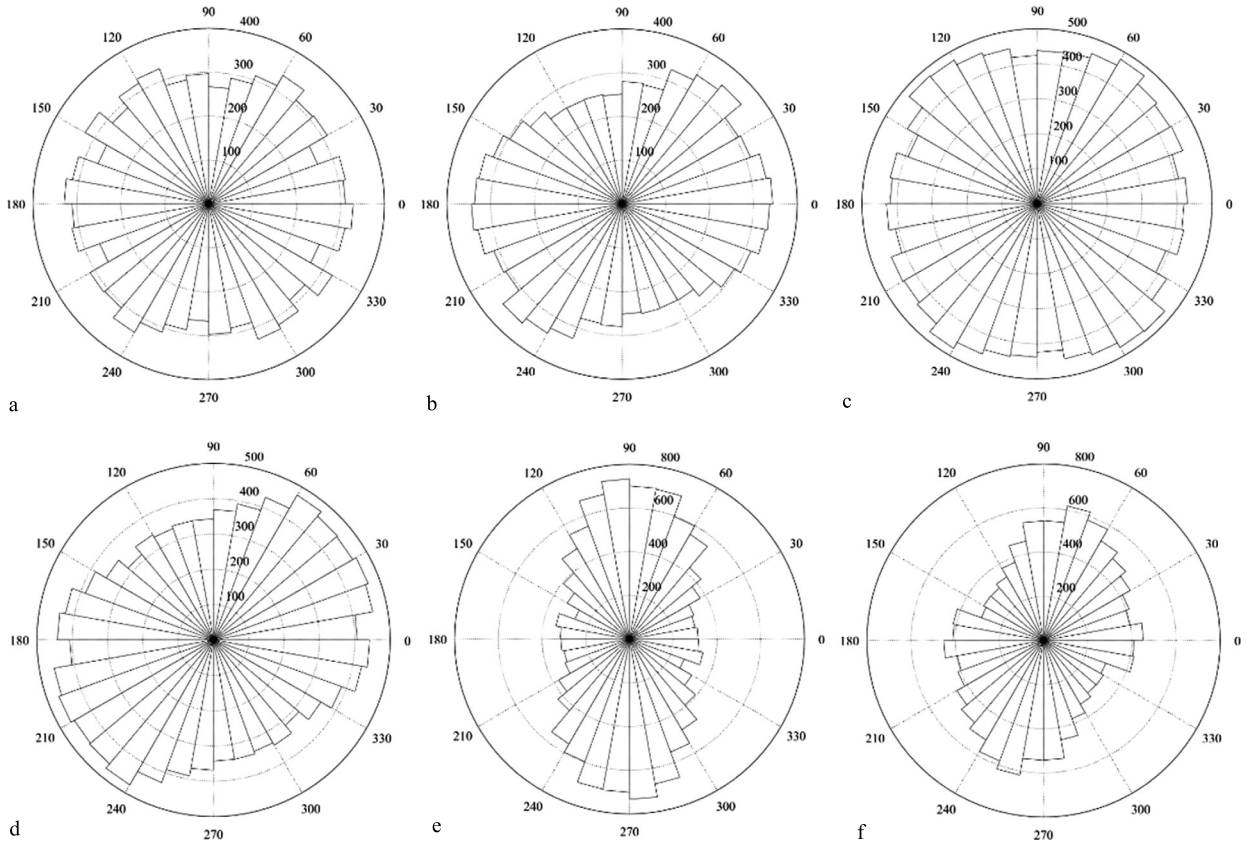

Fig. 12. Rose diagrams of contact orientation under a vertical stress of 400 kPa: (a) initial state of the circular grains; (b) ultimate state of the circular grains; (c) initial state of the triangular grains; (d) ultimate state of the triangular grains; (e) initial state of the elongated grains; (f) ultimate state of the elongated grains.

and

$$\sin\psi = \frac{\dot{\varepsilon_1} + \dot{\varepsilon_3}}{\dot{\varepsilon_1} - \dot{\varepsilon_3}}, \qquad \sin\varphi = \frac{\sigma_1 - \sigma_3}{\sigma_1 + \sigma_3} \tag{9}$$

In Equation (8), φ_c is the critical state friction angle, $\sin\psi$ and $\sin\varphi$ are calculated by Equation (9), and Δ is the non-coaxiality angle equal to the difference between the directions of the principal stress and of the principal strain rate.

4.1. Non-coaxial Rowe's stress–dilatancy relation used in the direct shear test

Fig. 17 illustrates Mohr's circle for the state of stress in the direct shear test. From the Mohr-circle for stress, the following relationship can be obtained:

$$\sin\varphi = \frac{\sigma_1 - \sigma_3}{\sigma_1 + \sigma_3} = 2t \Big/ \left[2\left(\frac{t\sin 2\alpha}{\tan\varphi_{ds}} + t\cos 2\alpha - t \right) + 2t \right] = \frac{\tan\varphi_{ds}}{\sin 2\alpha - \cos 2\alpha \tan\varphi_{ds}} \tag{10}$$

where the shear angle, φ_{ds}, can be now calculated using the vertical stress and shear stress values (Eq. (11)). Ochiai [49] has introduced the principal stress direction α (Eq. (12)):

$$\tan\varphi_{ds} = \tau'/\sigma_N \tag{11}$$

and

$$\tan\varphi_{ds} = \sin\varphi_c \tan\alpha \tag{12}$$

Fig. 18 illustrates the state of strain under direct shear conditions. $\sin\psi$ can be calculated as Eq. (9) if the principal strain is obtained as follows:

$$\varepsilon_1 + \varepsilon_3 = \varepsilon_{yy} \tag{13}$$

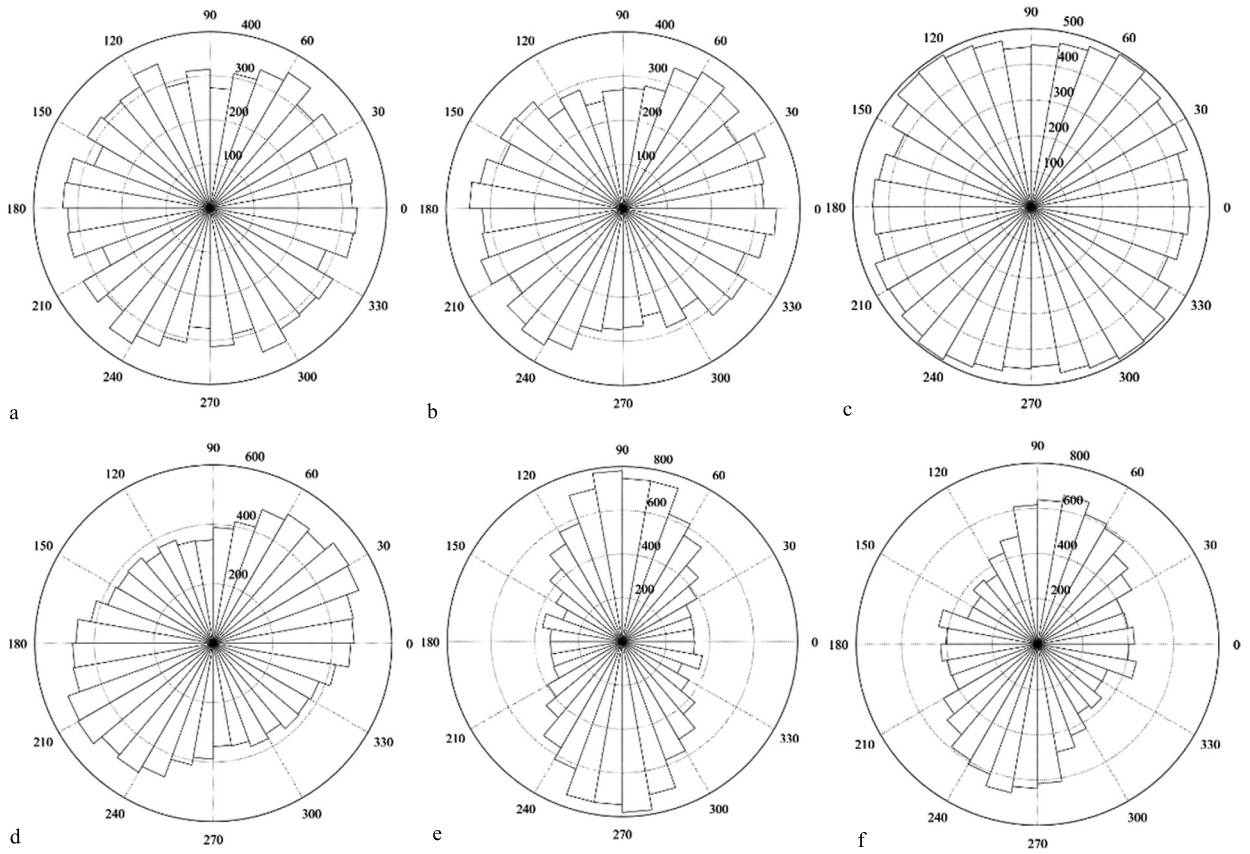

Fig. 13. Rose diagrams of contact orientation under a vertical stress of 600 kPa: (a) initial state of the circular grains; (b) ultimate state of the circular grains; (c) initial state of the triangular grains; (d) ultimate state of the triangular grains; (e) initial state of the elongated grains; (f) ultimate state of the elongated grains.

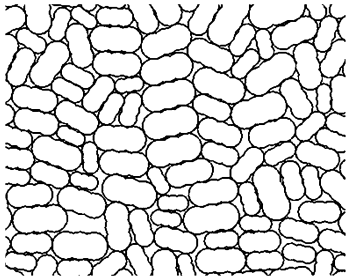

Fig. 14. Local amplifying diagram of the elongated particles in the initial state.

and

$$\varepsilon_1 - \varepsilon_3 = \sqrt{\varepsilon_{yy}^2 + \gamma_{xy}^2} \tag{14}$$

where ε_{yy} is the vertical strain, γ_{xy} is the shear strain.

Gutierrez et al. [48,50] introduced a method to calculate the non-coaxiality angle, defined as:

$$\Delta = \zeta - \alpha + \frac{1}{2}\sin^{-1}\left[\frac{\sin\varphi}{\sin\varphi_p}\sin(2\alpha - 2\zeta)\right] \tag{15}$$

and

$$\tan 2\zeta = -\sin\varphi_c / \tan\varphi_{ds} \tag{16}$$

In Eq. (15), φ_p is the peak friction angle, ζ is calculated as in Eq. (16).

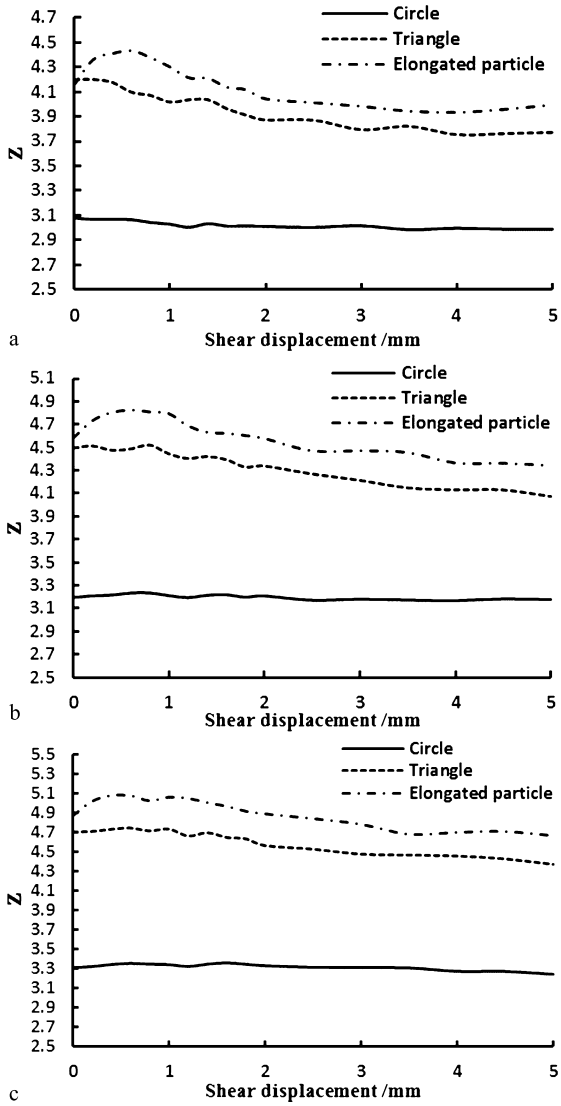

Fig. 15. Evolution of the coordination numbers of the granular materials: (a) vertical stress of 200 kPa; (b) vertical stress of 400 kPa; (c) vertical stress of 600 kPa.

4.2. Modifying the Rowe's stress–dilatancy relation

Rowe [51] has explored the variations of the minimum energy ratio $\overline{E}_{\min}$ with the angle of friction between particles. Such an angle varies with the different particle shapes and relative densities.

If φ_c is constant in Eq. (8), the theoretical line of stress–dilatancy will be far from the numerical data and cannot reflect the trend of the numerical data correctly, as illustrated in Fig. 19. A new relation is considered, where parameters OR and Z are used to reflect the impact of both particle shape and relative density on φ_c. Thus, the parameters OR and Z are considered to modify φ_c, and a modified stress–dilatancy relation is proposed:

$$\cos 2\Delta \sin\psi = \frac{(\sin\varphi_c)^{(OR_0-OR+Z_0-Z)} - \sin\varphi}{1-\sin\varphi(\sin\varphi_c)^{(OR_0-OR+Z_0-Z)}} \tag{17}$$

where the constant coefficient, OR_0, is 2.1 (this is a fitted parameter), and Z_0 is the coordination number in initial state of specimen (for circular particles, $Z_0 = 3.08$; for triangular particles, $Z_0 = 4.20$; for elongated particles, $Z_0 = 4.16$). Fig. 19 illustrates the comparisons of solutions according to Eqs. (17) and (8) as well as to numerical data. The modified theoretical lines of stress–dilatancy are close to the numerical data when the particle shape varies, and the slope of the modified theoretical line gradually decreases to zero, which is consistent with the trend of the numerical data.

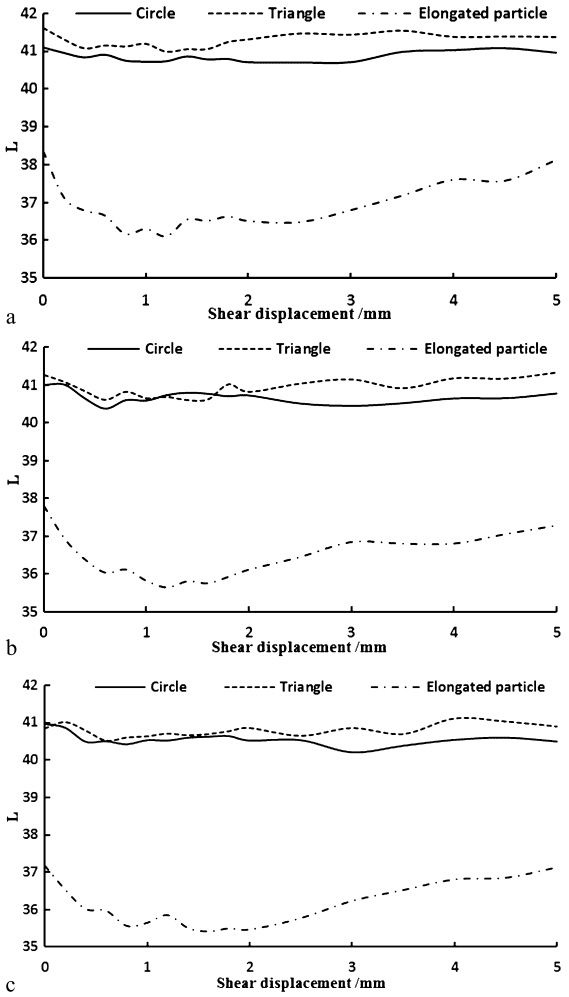

Fig. 16. Average path length evolution of granular materials: (a) vertical stress of 200 kPa; (b) vertical stress of 400 kPa; (c) vertical stress of 600 kPa.

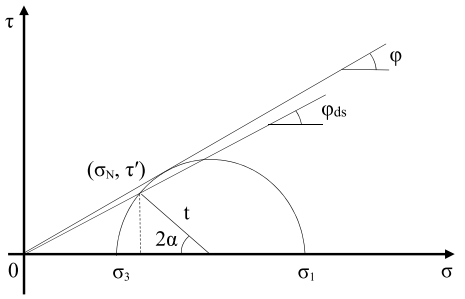

Fig. 17. Mohr's circle for the state of stress in a direct shear test.

5. Conclusions

In this paper, a two-dimensional DEM simulation is presented to explore the macromechanical properties and the microstructure evolution of different granular materials which are made up of circular, triangular and elongated particles, respectively. Finally, a modified Rowe's stress–dilatancy relation is proposed considering the overall regularity (OR) and the coordination number (Z). The conclusions can be inferred as follows.

(1) The particle shape has a remarkable influence on the mechanical properties of granular materials. With increasing the particles' regularity, the specimen is compressed more easily. In other word, the specimen has larger maximum and

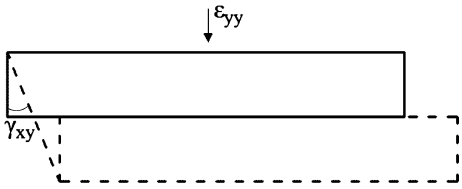

Fig. 18. State of strain under direct shear conditions.

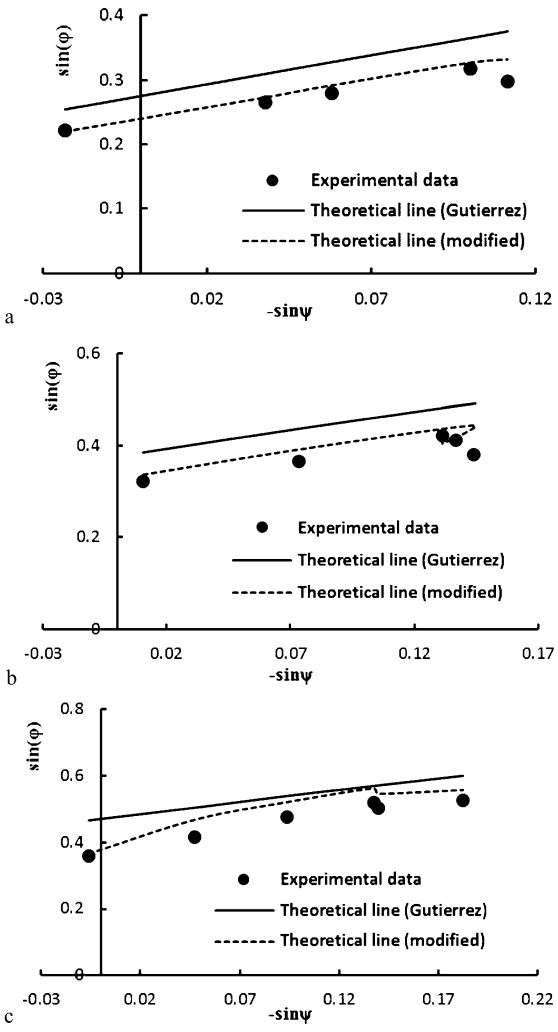

Fig. 19. Predicted and numerical data in the stress–dilatancy equation: (a) samples with circular particles; (b) samples with triangular particles; (c) samples with elongated particles.

minimum porosities. On the other hand, the peak shear stress ratio, the ultimate shear stress ratio, and the ultimate dilatancy increase when decreasing the value of *OR*.

(2) The characteristics of particle rotation in specimens are different according to particle shapes. At the ultimate state, the distribution of the average particle rotation along the specimen's height are similar when particle shapes are different. But near the shear plane zone, the more regular the particles are, the larger the value of average particle rotation is. And the variation of the maximum particle rotation for the three types of granular materials with particle shape is such that the maximum particle rotation increases when the parameter *OR* increases.

(3) The particle shape also has a remarkable influence on fabric evolution. In the initial state, the specimen with elongated particles is anisotropic and this value of anisotropy decreases when increasing the shear displacement. On the contrary, in the initial state, the specimen with triangular or circular particles has little anisotropy, and this value of anisotropy increases with increasing shear displacement. On the other hand, the Z value of specimen with circular particles is

smaller than that of specimens with irregular particle at the initial state, and for all the specimens with different particle shapes, the values of Z tend to decrease during the loading process.

(4) In this paper, the average path length (*APL*) is used to describe the connectivity (i.e. the structure) of networks for three types of assemblies. By combining the evolution of Z, it can be seen that the elongated particles are different from the isotropic particles (i.e. circular and triangular particles) on the structure and contact scales. The circular particle is similar to the triangular particle when structure is talked about, but the contact information displays remarkable differences between circular and triangular particles.

(5) The non-coaxial version of Rowe's stress–dilatancy relation cannot predict the trend of numerical data very well. Such theory is modified with parameters OR and Z. Finally, the modified stress–dilatancy relation can predict the trend of different particle shapes relatively well.

Acknowledgements

The authors appreciate the funding provided by the CAS Pioneer Hundred Talents Program (Dr. Liu Enlong) and the National Key Research and Development Program of China (Project No. 2017YFC1501003).

References

[1] J. Yang, X.D. Luo, Exploring the relationship between critical state and particle shape for granular materials, J. Mech. Phys. Solids 84 (2015) 196–213.
[2] C. Nouguier-Lehon, Effect of the grain elongation on the behaviour of granular materials in biaxial compression, C. R. Mecanique 338 (2010) 587–595.
[3] D. Höhner, S. Wirtz, V. Scherer, A study on the influence of particle shape on the mechanical interactions of granular media in a hopper using the Discrete Element Method, Powder Technol. 278 (2015) 286–305.
[4] S. Zhao, X. Zhou, Effects of particle asphericity on the macro- and micro-mechanical behaviors of granular assemblies, Granul. Matter 19 (2017) 38, https://doi.org/10.1007/s10035-017-0725-6.
[5] Y. Yang, Y.M. Cheng, Q.C. Sun, The effects of rolling resistance and non-convex particle on the mechanics of the undrained granular assemblies in 2D, Powder Technol. 318 (2017) 528–542.
[6] K. Shinohara, M. Oida, B. Golman, Effect of particle shape on angle of internal friction by triaxial compression test, Powder Technol. 107 (2000) 131–136.
[7] G.C. Cho, J. Dodds, J.C. Santamarina, Particle shape effects on packing density, stiffness, and strength: natural and crushed sands, J. Geotech. Geoenviron. Eng. 132 (2006) 591–602.
[8] J. Yang, L.M. Wei, Collapse of loose sand with the addition of fines: the role of particle shape, Géotechnique 62 (2012) 1111–1125.
[9] J. Reimann, J. Vicente, E. Brun, C. Ferrero, Y. Gan, A. Rack, X-ray tomography investigations of mono-sized sphere packing structures in cylindrical containers, Powder Technol. 318 (2017) 471–483.
[10] M. Goudarzy, D. König, T. Schanz, Small strain stiffness of granular materials containing fines, Soil Found. 56 (2016) 756–764.
[11] M. Oda, A mechanical and statistical model of granular material, Soil Found. 14 (1974) 13–27.
[12] P.A. Cundall, O.D.L. Strack, A discrete numerical model for granular assemblies, Géotechnique 29 (1979) 47–65.
[13] L. Cui, C. O'Sullivan, Exploring the macro- and micro-scale response of an idealized granular material in the direct shear apparatus, Géotechnique 56 (2006) 455–468.
[14] C. Nouguier-Lehon, B. Cambou, E. Vincens, Influence of particle shape and angularity on the behaviour of granular materials: a numerical analysis, Int. J. Numer. Anal. Methods 27 (2003) 1207–1226.
[15] S. Zhao, X. Zhou, W. Liu, Discrete element simulations of direct shear tests with particle angularity effect, Granul. Matter 17 (2015) 793–806.
[16] A.A. Peña, A. Lizcano, F. Alonso-Marroquin, H.J. Herrmann, Biaxial test simulations using a packing of polygonal particles, Int. J. Numer. Anal. Methods 32 (2008) 143–160.
[17] W.M. Yan, Fabric evolution in a numerical direct shear test, Comput. Geotech. 36 (2009) 597–603.
[18] S. Zhao, N. Zhang, X. Zhou, L. Zhang, Particle shape effects on fabric of granular random packing, Powder Technol. 320 (2017) 175–186.
[19] A. Tordesillas, P. O'Sullivan, D.M. Walker, Paramitha, Evolution of functional connectivity in contact and force chain networks: feature vectors, k-cores and minimal cycles, C. R. Mecanique 338 (2010) 556–569.
[20] D.M. Walker, A. Tordesillas, Topological evolution in dense granular materials: a complex networks perspective, Int. J. Solids Struct. 47 (2010) 624–639.
[21] C. Thornton, D.J. Barnes, Computer simulated deformation of compact granular assemblies, Acta Mech. 64 (1986) 45–61.
[22] M.R. Kuhn, Micro-mechanics of fabric and failure in granular materials, Mech. Mater. 42 (2010) 827–840.
[23] R. Wang, P. Fu, J.M. Zhang, Y.F. Dafalias, Evolution of various fabric tensors for granular media toward the critical state, J. Eng. Mech. 143 (2017) 04017117.
[24] N.P. Kruyt, Micromechanical study of fabric evolution in quasi-static deformation of granular materials, Mech. Mater. 44 (2012) 120–129.
[25] F. Nicot, L. Sibille, P.Y. Hicher, Micro–macro analysis of granular material behavior along proportional strain paths, Contin. Mech. Thermodyn. 27 (2015) 173–193.
[26] C.S. Chang, P.Y. Hicher, An elasto-plastic model for granular materials with microstructural consideration, Int. J. Solids Struct. 42 (2005) 4258–4277.
[27] J. Zhao, M. Jiang, K. Soga, S. Luding, Micro origins for macro behavior in granular media, Granul. Matter 18 (2016) 59.
[28] F. Altuhafi, C. O'Sullivan, I. Cavarretta, Analysis of an image-based method to quantify the size and shape of sand particles, J. Geotech. Geoenviron. Eng. 139 (2013) 1290–1307.
[29] L. Rothenburg, R.J. Bathurst, Analytical study of induced anisotropy in idealized granular materials, Géotechnique 39 (1989) 601–614.
[30] L. da, F. Costa, F.A. Rodrigues, G. Travieso, P.R. Villas Boas, Characterization of complex networks: a survey of measurements, Adv. Phys. 56 (2007) 167–242.
[31] S. Sheng, Y. Dou, X. Tao, S. Zhu, B. Xu, Q. Li, X. Guo, X. He, Specification of Soil Test SL237-1999 ed., China Water and Power Press, Beijing, 1999.
[32] A.A. Mirghasemi, L. Rothenburg, E.L. Matyas, Influence of particle shape on engineering properties of assemblies of two-dimensional polygon-shaped particles, Géotechnique 52 (2002) 209–217.
[33] GDR-MiDi, On dense granular flows, Eur. Phys. J. E 14 (2004) 341–365.
[34] F. Radjai, Force and fabric states in granular media, AIP Conf. Proc. 1145 (2009) 35–42.
[35] D.-H. Nguyen, E. Azéma, P. Sornay, F. Radjai, Effects of shape and size polydispersity on strength properties of granular materials, Phys. Rev. E 91 (2015) 032203.
[36] C. O'Sullivan, Particulate Discrete Element Modelling, first ed., Spon Press, Oxon, 2011.
[37] C. Thornton, L. Zhang, Numerical simulation of the direct shear test, Chem. Eng. Technol. 26 (2003) 153–156.

[38] J. Kozicki, M. Niedostatkiewicz, J. Tejchman, H.B. Muhlhaus, Discrete modelling results of a direct shear test for granular materials versus FE results, Granul. Matter 15 (2013) 607–627.
[39] D.M. Mueth, G.F. Debregeas, G.S. Karczmar, P.J. Eng, S.R. Nagel, H.M. Jaeger, Signatures of granular microstructure in dense shear flows, Nature 406 (2000) 385–389.
[40] D. Vågberg, P. Olsson, S. Teitel, Shear banding, discontinuous shear thickening, and rheological phase transitions in athermally sheared frictionless disks, Phys. Rev. E 95 (2017) 052903.
[41] Z. Zhang, L. Chen, S. Zhou, L. Fang, J. Guan, T. Zou, Analytical solution of average path length for Apollonian networks, Phys. Rev. E 77 (2008) 017102.
[42] Y.Y. Liu, J.J. Slotine, A.L. Barabási, Controllability of complex networks, Nature 473 (2011) 167–173.
[43] J. Gao, B. Barzel, A.L. Barabási, Universal resilience patterns in complex networks, Nature 530 (2016) 307–312.
[44] R. Bond, Complex networks: network healing after loss, Nat. Hum. Behav. 1 (2017) 87.
[45] A. Ahmed, A. Thomo, Computing source-to-target shortest paths for complex networks in RDBMS, J. Comput. Syst. Sci. 89 (2017) 114–129.
[46] A. Gozzard, M. Ward, A. Datta, Converting a network into a small-word network: fast algorithms for minimizing average path length through link addition, Inf. Sci. 422 (2018) 282–289.
[47] P.W. Rowe, The stress–dilatancy relation for static equilibrium of an assembly of particles in contact, Proc. R. Soc. Lond. Ser. A 269 (1962) 500–527.
[48] M. Gutierrez, J. Wang, Non-coaxial version of Rowe's stress–dilatancy relation, Granul. Matter 11 (2009) 129–137.
[49] H. Ochiai, The behaviour of sand in the direct shear test, Soil Found. 15 (1975) 93–100.
[50] M. Gutierrez, K. Ishihara, I. Towhata, Flow theory for sand during rotation of principal stress direction, Soil Found. 31 (1991) 121–132.
[51] P.W. Rowe, Theoretical meaning and observed values of deformation parameters for soil, in: Proceedings of The Roscoe Memorial Symposium, Cambridge University, 1971, pp. 143–194.